

Multiferroic Properties of BaFe₁₂O₁₉ Ceramics

*Xiuna Chen, Guolong Tan **

*State Key Laboratory of Advanced Technology for Materials Synthesis and Processing,
Wuhan University of Technology, Wuhan 430070, China*

Abstract

Simultaneous occurrence of big ferroelectricity and strong ferromagnetism has been observed in Barium Hexaferrite ceramics. Barium hexaferrite (BaFe₁₂O₁₉) powders with hexagonal crystal structure have been successfully synthesized by polymer precursor method using barium acetate and ferric acetylacetonate as the precursor. The powders were pressed into pellets, which were sintered into ceramics at 1100°C~1300°C for 1 hour. The structure and morphology have been determined by X-ray diffraction (XRD) and field emission scanning electron microscopy (FESEM). Large spontaneous polarization was observed in the BaFe₁₂O₁₉ ceramics at room temperature, exhibiting a clear ferroelectric hysteresis loop. The maximum remanent polarization of BaFe₁₂O₁₉ ceramic is estimated to be $P_r \sim 11.8 \mu\text{C}/\text{cm}^2$. The FeO₆ octahedron in its perovskite-like hexagonal unit cell as well as the shift of Fe³⁺ off the center of octahedron are proposed to be the origin of polarization in BaFe₁₂O₁₉. The BaFe₁₂O₁₉ ceramic also shows strong ferromagnetism at room temperature.

Keywords: BaFe₁₂O₁₉, Multiferroic, Ferroelectric Properties, Ferromagnetic properties, Functional applications.

I Introduction

In recent years, there has been increasing interest in multiferroic materials, they provide a wide range of potential applications such as multiple-state memory elements, novel memory media, transducers and new functional sensors^{1, 2}. However, the materials in which ferroelectricity and ferromagnetism coexist are rare^{3, 4} and mostly exhibit rather weak ferromagnetism. Because the room-temperature multiferroism is essential to the realization of multiferroic devices that exploit the coupling between ferroelectric and ferromagnetic

* Corresponding author; Tel: +86-27-87870271; fax: +86-27-87879468. Email address: gltan@whut.edu.cn

orders at ambient conditions, BiFeO₃ together with more recently revealed LuFe₂O₄, Pb₂Fe₂O₅ and PbFe₁₂O₁₉^{5, 6, 7, 8, 9} are currently considered to be promising candidates for practical device applications. The perovskite BiFeO₃ exhibits weak magnetism, which could somehow prevent its practical application. Therefore preparation of a material in which large ferroelectricity and strong ferromagnetism coexist would be a milestone for modern electrics and functionalized materials¹⁰. As large ferroelectric polarization was found in PbFe₁₂O₁₉ ceramics⁹ with hexagonal structure, it opens up a new direction for potential multiferroic candidate in such traditional ferromagnetic oxides as BaFe₁₂O₁₉ which holds similar perovskite-like lattice units in its hexagonal structure.

M-type hexaferrites denoted as BaFe₁₂O₁₉ has attracted a lot of attention because of their excellent magnetic properties and potential application in various fields.¹¹ As a hexaferrite, BaFe₁₂O₁₉ is one of the mostly used ferrites in applications as permanent magnets¹². The magnetization per formula unit at 0K is (8-4)×5=20μB.¹³ Due to its excellent magnetic properties, BaFe₁₂O₁₉ could hold a great promise to be a good applicable Pb-free multiferroic candidate in case suitable ferroelectricity could be observed.

Magnetic field induced electric polarization has been observed in BaFe_{12-x}Sc_xMg_δO₁₉ (δ=0.05) at 10K¹⁴. However, the multiferroic aspect of pure BaFe₁₂O₁₉ has never been studied yet. In this paper we are going to present large multiferroic effect in BaFe₁₂O₁₉ compound. The fabrication of BaFe₁₂O₁₉ powders by a polymer precursor method as well as the large spontaneous polarization of BaFe₁₂O₁₉ ceramic in addition to its strong ferromagnetism at room temperature will also be presented.

II Experimental procedure

Barium hexaferrite “BaFe₁₂O₁₉” powders were prepared by polymer precursor method using barium acetate (Ba(CH₃COO)₂) and ferric acetylacetonate as the starting materials. Typically, 0.2580 g barium acetate was dissolved in 15 mL distilled water to form a clear solution. The solution was stored in a three neck glass bottle. In order to prevent the hydrolysis of ferric acetylacetonate, the following experiments were carried out in the glove box. 3.7082g ferric acetylacetonate was dissolved in 200mL benzene. The prepared barium acetate solution and the ferric acetylacetonate in benzene, under the stoichiometric atomic

ratio of Ba/Fe=1/10.5 was continuously heated and stirred in order to induce a homogenous mixture of both solutions at 50°C for 1 hour. Then, 100ml ammonia and 15ml polyethylene glycol mixture solution was added into the above solution, thus a colloid dispersion solution was formed. The dispersion solution was maintained at 323K with stirring for 8 hours. Afterwards, the colloid solution was moved out of the glove box. The water and organic solution were removed by centrifugation. the remaining colloid powders were calcined at 450 °C for 1.5h to completely remove the organic part. 0.10g powders were weighted and pressed into pellet, which was then sintered into ceramics at 1200°C and 1300°C for 1 hour, respectively. Phase identification was performed by X-ray powder diffraction (XRD) method with Cu K α radiation. The images for the morphology and microstructure of the ceramics were collected by S-4800 field emission scanning electron microscopy. All the sintered samples should be polished and both surfaces of samples were coated with silver paste as electrodes for P-E hysteresis loop measurement. The ferroelectric hysteresis loop was measured using a home-made instrument, termed as ZT-IA ferroelectric measurement system. The magnetization of the samples was measured using a Quantum Design physical property measurement system (PPMS).

III Results and discussion

(1). Structure and microstructure of BaFe₁₂O₁₉ ceramics

The XRD patterns of the BaFe₁₂O₁₉ powders being calcined at 1200°C and 1300°C, respectively, are shown in *Figure 1*, which showed the hexagonal structure of pure BaFe₁₂O₁₉ in single phase. The XRD patterns of BaFe₁₂O₁₉ powders demonstrate the magnetoplumbite structure with no extra reflections and is perfectly indexed to (110), (112), (107), (114) , (200), (203) and (2,0,11) crystal plane of hexagonal BaFe₁₂O₁₉ (PDF# 43-0002). The relative intensities of (107) and (114) peaks, which correspond to the inclined c-axis orientation, are higher than those of (112) and (200) peaks. These results indicate that the grains of BaFe₁₂O₁₉ ceramics are randomly oriented.

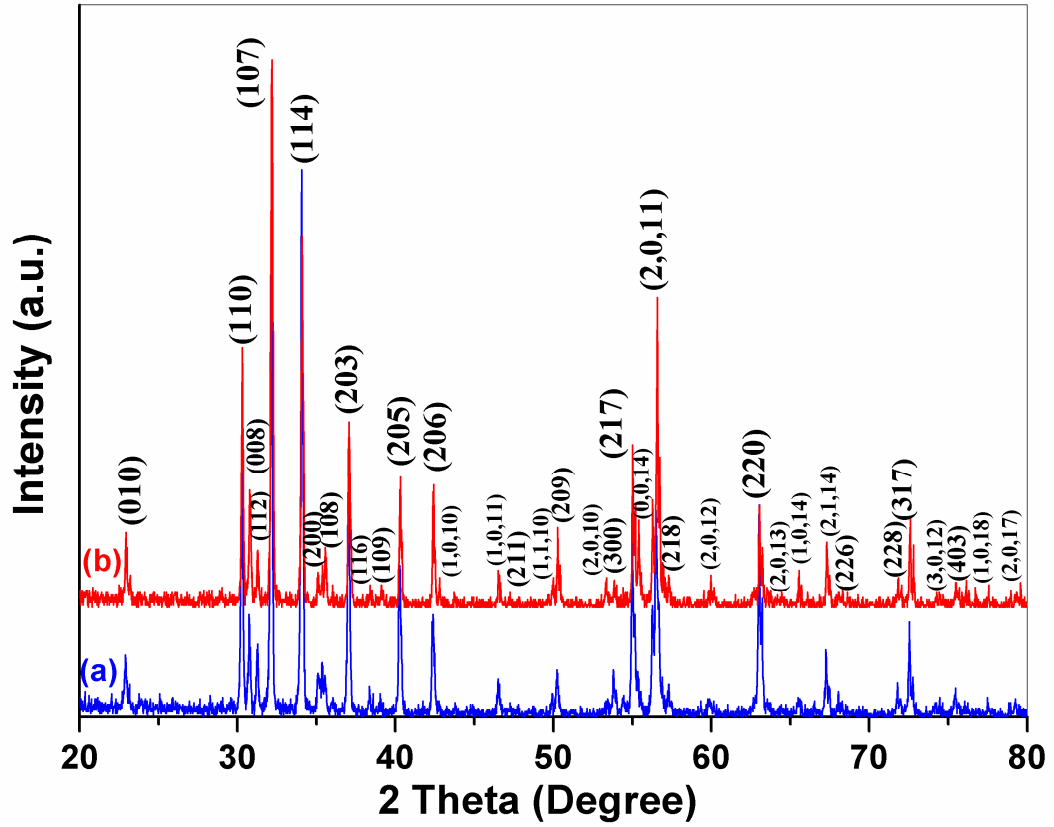


Figure 1: XRD pattern of the $\text{BaFe}_{12}\text{O}_{19}$ powders being calcined at (a) $1200\text{ }^{\circ}\text{C}$ and (b) $1300\text{ }^{\circ}\text{C}$, respectively.

Figure 2 (a) and (b) show two FESEM images of $\text{BaFe}_{12}\text{O}_{19}$ ceramic being sintered at $1200\text{ }^{\circ}\text{C}$ for one hour. The image clearly shows that the $\text{BaFe}_{12}\text{O}_{19}$ grains appear the hexagonal plate-like shape with the random orientation, and the grain size of $\text{BaFe}_{12}\text{O}_{19}$ ceramic is estimated to be less than $1\text{ }\mu\text{m}$. Figure 1 (c) and (d) exhibit two FESEM images for the $\text{BaFe}_{12}\text{O}_{19}$ ceramic being sintered at $1300\text{ }^{\circ}\text{C}$ for one hour. It can be seen that $\text{BaFe}_{12}\text{O}_{19}$ grains take plate-like shape, the grain size of which is among the range of $2\sim 10\text{ }\mu\text{m}$. Its densification has much more improved in comparison with that being sintered at $1200\text{ }^{\circ}\text{C}$. Therefore, with the increase of sintering temperature, there is a great growth in grain size and improvement in densification for the $\text{BaFe}_{12}\text{O}_{19}$ ceramics. The distorted hexagonal flaky grains are frequently observed in the $\text{BaFe}_{12}\text{O}_{19}$ ceramics, as being shown in Figure 2. Cylinder shaped grains can also be found in the SEM images. EDX measurement indicates that Ba rich phase has deposited onto the grain boundary area in $\text{BaFe}_{12}\text{O}_{19}$ ceramics through liquid phase sintering process, which expedites the rapid growth of the grain size of the ceramics. The hexahedron shaped grains are consistent with the hexagonal symmetry of BFO crystal. $[0001]$ direction is normal to the surface of the flaky

grains. The flaky shape suggests that the grains did not take priority growth along with [0001] direction but with [0100] direction. Obviously the growth rate of the grains along with [0100] direction is much faster than that along with other directions. Thus the grains did not take perfect hexahedron shapes, but actually the deformed flaky ones.

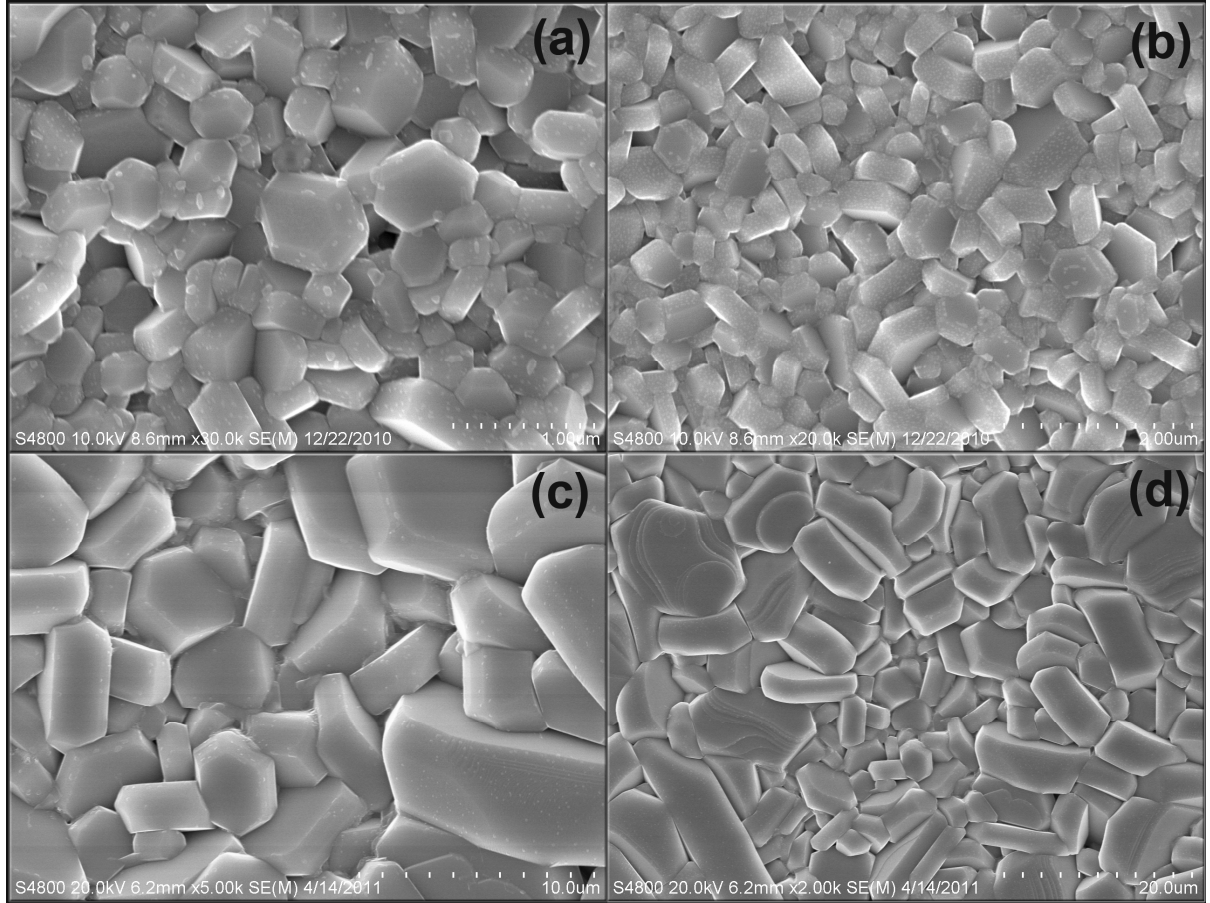


Figure 2: FESEM images of $BaFe_{12}O_{19}$ ceramics being sintered at (a), (b) 1200 °C and (c), (d) 1300 °C for 1h.

(2) Ferroelectric properties of $BaFe_{12}O_{19}$ ceramics

Ferroelectric properties were characterized using polarization hysteresis and pulse polarization measurements. The electric field-induced polarization behavior was examined using a home-made ferroelectric measurement system termed as ZT-IA. During the ferroelectric measurement, the specimen was parallel connected with a capacitor of 0.1 μ F for compensation. The F-E measurement was carried out by a tri-angular wave voltage. Evidence for the characterization of ferroelectric state of $BaFe_{12}O_{19}$ ceramic is provided in Figure 3, which shows polarization cycles exhibiting clear ferroelectric hysteresis loops in $BaFe_{12}O_{19}$ ceramics under applied electric fields of different amplitudes obtained at room

temperature. The maximum remanent polarization (P_r) and the coercive electric field (E_c) obtained from the ferroelectric hysteresis loop in *Figure 3 (a)* are $\sim 11.8\mu\text{C}/\text{cm}^2$ and $\sim 5.8\text{kV}/\text{m}$, respectively, for the $\text{BaFe}_{12}\text{O}_{19}$ ceramic being sintered at 1200°C for 1 hour.

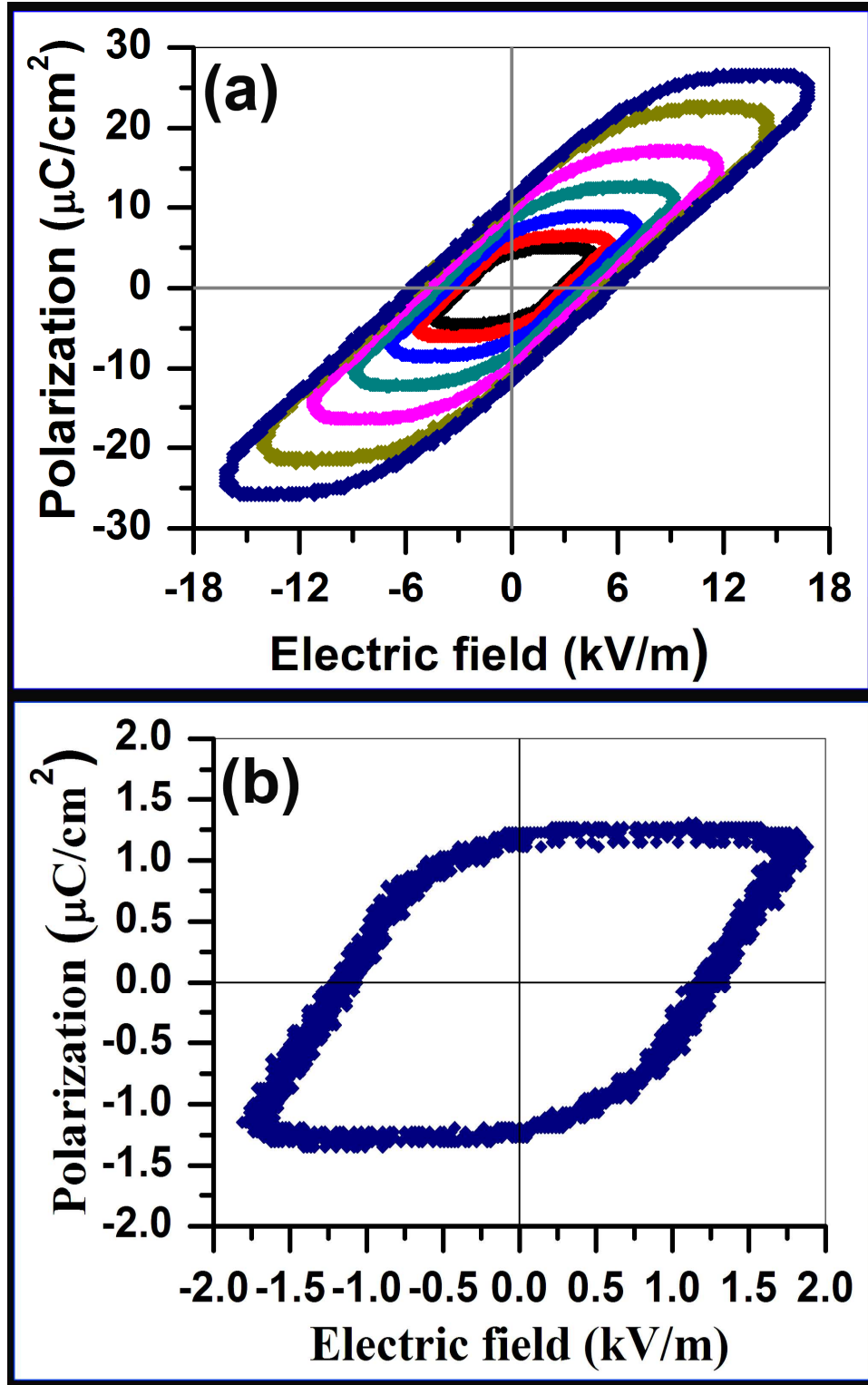


Figure 3: Ferroelectric hysteresis loops of $\text{BaFe}_{12}\text{O}_{19}$ ceramic being sintered at (a) 1200°C and (b) 1300°C for 1h, respectively.

After $\text{BaFe}_{12}\text{O}_{19}$ ceramic has been sintered at 1300°C for 1 hour, the grain size and

densification has been greatly improved in comparison with that being sintered at 1200 °C, as being seen from their SEM images in *Figure 2*. The polarization hysteresis loop for the BaFe₁₂O₁₉ ceramic being sintered at 1300°C exhibits a F-E loop being closer to the standard one, which saturates at a certain field and demonstrates some convex and concave regions in the curve, as being shown in *Figure 3* (b). The saturated polarization of the BaFe₁₂O₁₉ ceramics being sintered at 1300°C demonstrates a quick reduction with the increase of the densification and grain size. The maximum remanent polarization (P_r), the polarization maximum (P_{max}) and the coercive electric field (E_c) obtained from the ferroelectric hysteresis loop in *Figure 3* (b) are $\sim 1.2\mu\text{C}/\text{cm}^2$, $\sim 1.6\mu\text{C}/\text{cm}^2$ and $\sim 1.25\text{kV}/\text{m}$ respectively for BaFe₁₂O₁₉ ceramic pellet being sintered at 1300°C. Conclusion could be drawn from *Figure 3* (a) & (b) that the ferroelectricity is reduced with the increase of the sintering temperature due to the improvement of densification and growth of the grain size of the ceramics.

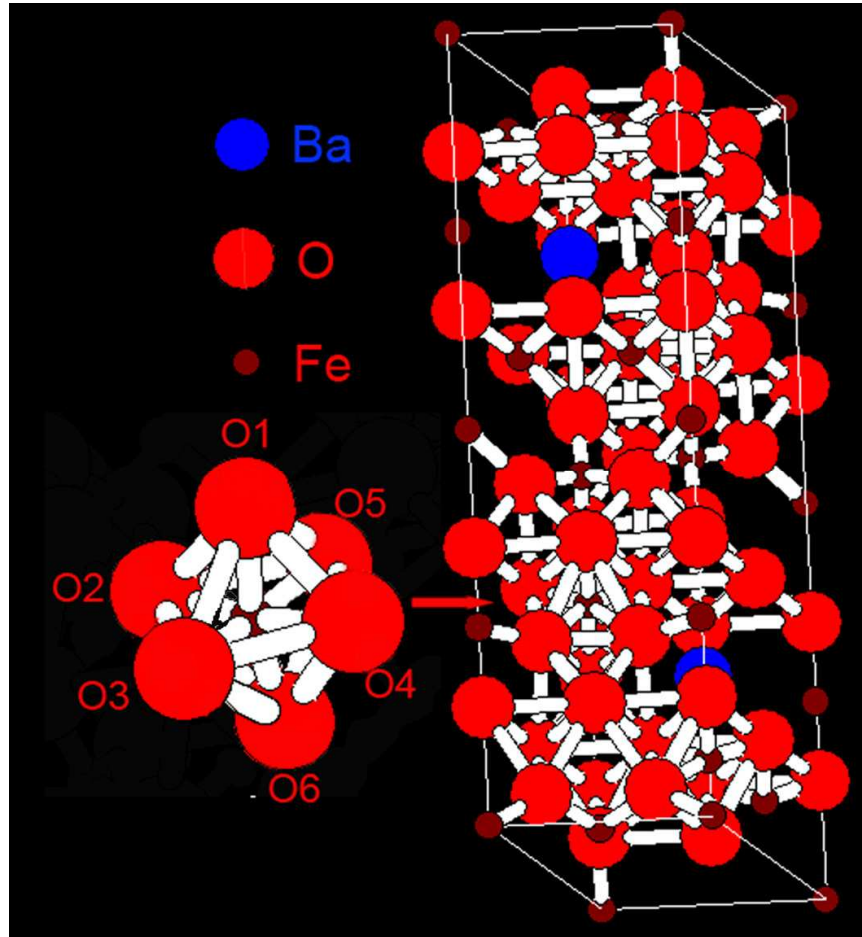


Figure 4: Crystal structure model of BaFe₁₂O₁₉ (ICSD #45442) and magnified FeO₆ octahedron perovskite structure found in the crystal structure model of BaFe₁₂O₁₉.

In order to understand the origin of the ferroelectricity of barium hexaferrite, we firstly investigated the crystal structure model of $\text{BaFe}_{12}\text{O}_{19}$ (ICSD #45442) with space group $P6_3/mmc$, which is exhibited in *Figure 4*. Careful analysis of the unit model structure suggests a perovskite-like crystal structure with one distorted FeO_6 oxygen octahedron in hexagonal $\text{BaFe}_{12}\text{O}_{19}$ as being shown in *Figure 4*. Each hexagonal $\text{BaFe}_{12}\text{O}_{19}$ model has one FeO_6 oxygen octahedron in a sub-unit cell. In a normal octahedron, Fe cation is located at the center of an octahedron of oxygen anions. However, in the unit cell of $\text{BaFe}_{12}\text{O}_{19}$ below the Curie temperature, there is also a distortion to a lower-symmetry phase accompanied by the shift off-center of the small Fe cation. Fe cation shifts away from the center along b axis, while O_5 and O_6 shifts off their original positions of octahedron along opposite directions of a-axis, which leads to the distortion of $\text{O}_5\text{-Fe-O}_6$ bond away from straight line. The spontaneous polarization derives largely from the electric dipole moment created by the two shifts, which induces the large ferroelectric hysteresis loops for $\text{BaFe}_{12}\text{O}_{19}$.

(3) Ferromagnetism of $\text{BaFe}_{12}\text{O}_{19}$ ceramics

$\text{BaFe}_{12}\text{O}_{19}$ is a kind of traditional ferromagnetic material, whose magnetization behavior has been widely studied. Magnetic properties of the $\text{BaFe}_{12}\text{O}_{19}$ sample being sintered at 1300°C were measured at room temperature with a Quantum Design physical property measurement system (PPMS). The field-dependent magnetization hysteresis loop for $\text{BaFe}_{12}\text{O}_{19}$ sample being sintered at 1300°C is shown in *Figure 5*. The remnant magnetic polarization (M_r) of the $\text{BaFe}_{12}\text{O}_{19}$ is 32 emu/g, the saturation magnetization is ~ 55 emu/g. The coercivity (H_c) of the $\text{BaFe}_{12}\text{O}_{19}$ sample is 1607 Oe. The magnetization of our $\text{BaFe}_{12}\text{O}_{19}$ sample is lower than the bulk value of 67.7 emu/g. Meanwhile, The $\text{BaFe}_{12}\text{O}_{19}$ sample being sintered at 1200°C exhibit reduced magnetization value in comparison with its counterpart being sintered at higher temperature (1300°C). According to the SEM observation, the grain size of the $\text{BaFe}_{12}\text{O}_{19}$ ceramic being sintered at 1200°C was less than $1\mu\text{m}$, while that being sintered at 1300°C was estimated to be among the range of $2\sim 10\mu\text{m}$. The particle size of $\text{BaFe}_{12}\text{O}_{19}$ sample grew very fast with sintering temperature. The reduction of the magnetization for $\text{BaFe}_{12}\text{O}_{19}$ samples with decreasing particle size was caused by the incomplete coordination of the atoms on the particle surface, leading to a noncollinear spin configuration, which causes the formation of a surface spin canting^{15, 16, 17},

and due to thermal fluctuation of magnetic moments, which significantly diminishes the total magnetic moment for a given magnetic field¹⁵.

Size effect plays an important role on the reduction of the magnetization of $\text{BaFe}_{12}\text{O}_{19}$ ceramics. Usually the so-called critical size determines the properties of magnetic materials^{18, 19, 20}. When particle size is smaller than this critical value, particles locate within one single domain; otherwise multiple-domain may occur in particles. As particles are larger than the single domain size for the ceramics being sintered at higher temperature, the domain walls become predominant. While the sintering temperature rises, the particle size increased towards to the critical single domain size, the coercivity increase and reach a maximum value at the single domain size because of the coherent rotation of spins.

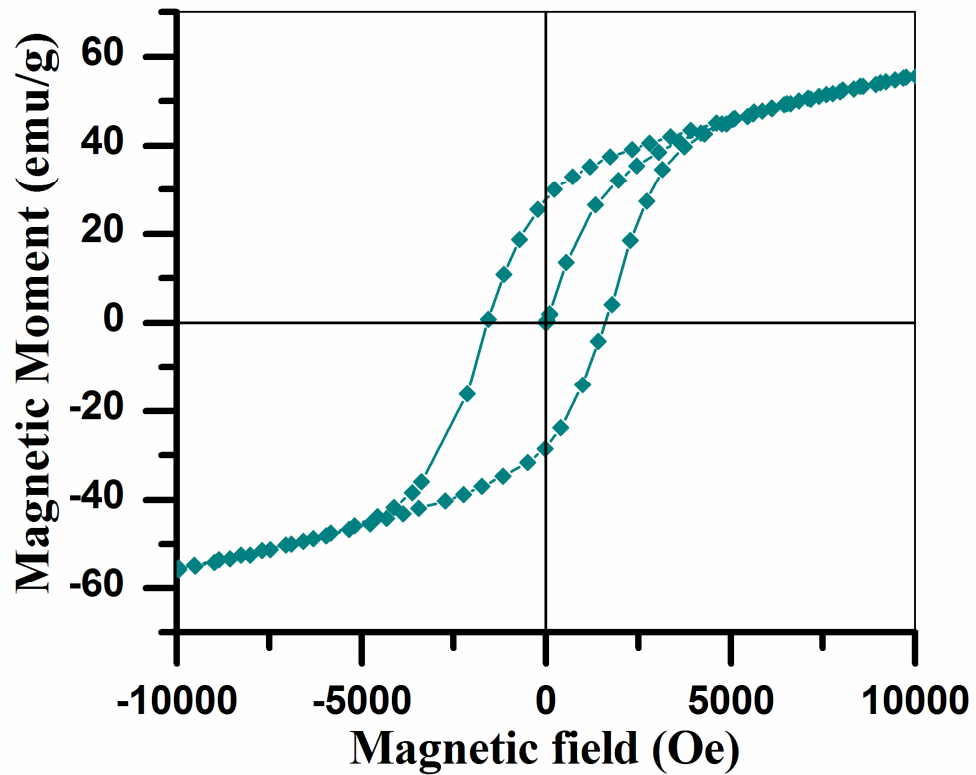


Figure 5 Magnetic hysteresis loop of the $\text{BaFe}_{12}\text{O}_{19}$ ceramics being sintered at 1300 °C.

So far, BiFeO_3 is the best-known multiferroic material, which also exhibits both ferromagnetic and ferroelectric ordering above room temperature. However, the weak ferromagnetism of BiFeO_3 may prevent its application²¹. In contrast, strong ferromagnetism and large ferroelectricity simultaneously occurred in $\text{BaFe}_{12}\text{O}_{19}$ ceramics above room temperature. The remnant magnetic polarization (M_r) and the magnetic coercivity (H_c) of BiFeO_3 was reported to be less than 0.1 emu/g and 200 Oe²¹, which are

much less than that of ~ 32 emu/g and 1607 Oe for $\text{BaFe}_{12}\text{O}_{19}$ ceramics. The remnant magnetic polarization of $\text{BaFe}_{12}\text{O}_{19}$ ceramics is 320 times higher than that of BiFeO_3 ceramics, while the magnetic coercivity (H_c) is around 8 times higher than that of BiFeO_3 ceramics. Meanwhile, as being mentioned above, the maximum remnant polarization (P_r) of $\text{BaFe}_{12}\text{O}_{19}$ ceramics is determined to be $\sim 32 \mu\text{C}/\text{cm}^2$, which is around 5.2 times higher than the reported value of $6.1 \mu\text{C}/\text{cm}^2$ from BiFeO_3 ceramics²². Therefore multiferroic $\text{BaFe}_{12}\text{O}_{19}$ ceramics have clear and unique advantage over the best multiferroic system of BiFeO_3 materials. This holds promise for its application in new generation of electronic devices as a applicable multiferroic candidate in single phase.

IV Conclusion

In summary, large ferroelectricity and strong ferromagnetism have been found in barium hexaferrite ceramics. pure barium hexaferrite ($\text{BaFe}_{12}\text{O}_{19}$) powders have been synthesized by a novel polymer precursor method using glycerin as solvent. The powders were pressed into pellets, which were sintered into ceramics at 1200°C and 1300°C for 1 hour, respectively. The ferroelectric hysteresis loop of the sample shows that the maximum remnant polarization (P_r) and the coercivity (H_c) are $11.8 \mu\text{C}/\text{cm}^2$ and $5.8 \text{ kV}/\text{m}$, respectively for $\text{BaFe}_{12}\text{O}_{19}$ ceramics being sintered at 1200°C . We propose that the source of polarization is the distortion of the Fe oxygen octahedron in the lattice unit of its perovskite-like hexagonal structure. The magnetic hysteresis loop of the sample shows that the remnant magnetic polarization (M_r) and the magnetic coercivity (H_c) are ~ 11.8 emu/g and 1632 Oe, respectively. These results clearly demonstrate the multiferroic characterization of the barium hexaferrite ceramics above room temperature.

Acknowledgement: The authors greatly acknowledge the financial support from the Natural Science Foundation of Hubei Province (2010CDA078) and

References

-
- ¹ Khomskii, D. I. *Journal of Magnetism and Magnetic Materials* 2006, 306 , 1.
 - ² Fiebig, M.; Lottermoser, Th.; Frohlich, D.; Goltsev, A. V.; Pisarev, R. V. ; *Nature* 2002, 419, 818.

-
- ³ Hill, N. A.; *J. Phys. Chem. B* 2000, 104, 6694.
- ⁴ Hur, N.; Park, S.; Sharma, P. A.; Ahn, J. S.; Guha, S.; Cheong, S. W.; *Nature* 2004, 429, 392.
- ⁵ Ikeda, N.; Ohsumi, H.; Ohwada, K.; Ishii, K.; Inami, T.; Kakurai, K.; Murakami, Y.; Yoshii, K.; Mori, S.; Horibe, Y.; Kito, H.; *Nature* 2005, 436, 1136.
- ⁶ Xiang, H. J.; Whangbo, M. H.; *Phys. Rev. Lett* 2007, 98, 246403.
- ⁷ Ryu, S.; Kim, J. Y.; Shin, Y. H.; Park, B. G.; Son, J. Y.; Jang, H. M.; *Chem. of Mater* 2009, 21, 5050.
- ⁸ Wang, M.; Tan, G. L.; *Mater. Res. Bull* 2011, 46, 438.
- ⁹ Tan, G. L.; Wang, M.; *J. Electroceramics* 2011, 26, 170.
- ¹⁰ Hemberger, J.; Lunkenheimer, P.; Fichtl, R.; Krug von nidda, H. A.; Tsurkan, V.; Loidl, A.; *Nature* 2005, 434, 364.
- ¹¹ Yang, N.; Yang, H. B.; Jia, J. J.; Pang, X. F.; *Journal of Alloys and Compounds* 2007, 438, 263.
- ¹² Diaz-Castañón, S.; Sánchez J. L.; Estevez-Rams, L. I.; Leccabue, F.; Watts, B. E.; *Journal of Magnetism and Magnetic Materials* 1998, 185, 194.
- ¹³ Chaudhury, S.; Rakshit, S. K.; Parida, S. C.; Ziley, S.; *Journal of Alloys and Compounds* 2008, 455, 25.
- ¹⁴ Tokunaga, Y.; Kaneko, Y.; Okuyama, D.; Ishiwata, S.; Arima, T.; Wakimoto, S.; Kakurai, K.; Taguchi, Y.; Tokura, Y.; *Phy. Rev. Lett.* 2010, 105, 257201.
- ¹⁵ Drofenik, M.; Ban, I.; Ferk, G.; Makovec, D.; Znidarsic, A.; Jaglicic, Z.; Lisjak, D.; *J. Am. Ceram. Soc* 2010, 93, 1602.
- ¹⁶ Coey, J. M. D.; *Phys. Rev. Lett* 1971, 27, 1140.
- ¹⁷ Kodama, R. H.; Berkowitz, A. E.; McNiff, E. J.; Foner, S.; *Phys. Rev. Lett* 1996, 77, 394.
- ¹⁸ Faloh, J. C.; Castañón, S. D.; Almodovar, N. S.; *J. Magn. Magn. Mater* 2000, 222, 271.
- ¹⁹ Jacabo, S. E.; Civalé, L.; Blesa, M. A.; *J. Magn. Magn. Mater* 2003, 260, 37.
- ²⁰ Ding, J.; Miao, W. F.; McCormick, P. G.; Street, R. J.; *J. Alloys Compd* 1998, 281, 32.
- ²¹ Wang, J.; Neaton, J. B.; Zheng, H.; Nagarajan, V.; Ogale, S. B.; Liu, B.; Viehland, D.; Vaithyanathan, V.; Schlom, D. G.; Waghmare, U. V.; Spaldin, N. A.; *Science* 2003, 299, 1719.
- ²² Faloh, J. C.; Castañón, S. D.; Almodovar, N. S.; *J. Magn. Magn. Mater* 2000, 222, 271.